Bioactive Materials 14 (2022) 389–401

Contents lists available at ScienceDirect

Bioactive Materials

journal homepage: www.keaipublishing.com/en/journals/bioactive-materials

A hydrogel spinal dural patch with potential anti-inflammatory, pain relieving and antibacterial effects

Jiahao Li [a,1], Jingjing Tian [b,1], Chunxu Li [a], Longyun Chen [c], Yu Zhao [a,*]

[a] Department of Orthopaedic Surgery, Peking Union Medical College Hospital, Chinese Academy of Medical Sciences and Peking Union Medical College, Beijing, China
[b] Medical Science Research Center, Peking Union Medical College Hospital, Chinese Academy of Medical Sciences and Peking Union Medical College, Beijing, China
[c] Department of Pathology, State Key Laboratory of Complex Severe and Rare Disease, Molecular Pathology Research Center, Peking Union Medical College Hospital, Chinese Academy of Medical Sciences and Peking Union Medical College, Beijing, China

ARTICLE INFO

Keywords:
Alginate hydrogel
Chitosan adhesive
Dural defect repair
Anti-inflammatory
Bacteriostasis

ABSTRACT

CSFL caused by spinal dural defect is a common complication of spinal surgery, which need repair such as suture or sealants. However, low intracranial pressure symptoms, wound infection and prolonged hospital associated with pin-hole leakage or loose seal effect were often occurred after surgical suture or sealants repair. Stable, pressure resistance and high viscosity spinal dural repair patch in wet environment without suture or sealants was highly needed. Herein, a bioactive patch composed of alginate and polyacrylamide hydrogel matrix cross-linked by calcium ions, and chitosan adhesive was proposed. This fabricated patch exhibits the capabilities of promoting defect closure and good tight seal ability with the bursting pressure is more than 790 mm H_2O in wet environment. In addition, the chitosan adhesive layer of the patch could inhibit the growth of bacterial *in vitro*, which is meaningful for the postoperative infection. Furthermore, the patch also significantly reduced the expression of GFAP, IBA-1, MBP, TNF-α, and COX-2 in early postoperative period *in vivo* study, exerting the effects of anti-inflammatory, analgesic and adhesion prevention. Thus, the bioactive patch expected to be applied in spinal dural repair with the good properties of withstanding high pressure, promoting defect closure and inhibiting postoperative infection.

1. Introduction

The spinal dura mater is a long tubular sac composed of dense connective tissue and serves as a sheath for the spinal cord and a tube for the cerebrospinal fluid [1]. Injury to the dura during spinal surgery is the direct cause of cerebrospinal fluid leakage (CSFL) [2,3]. CSFL is associated with a cascade of adverse outcomes, such as low intracranial pressure symptoms, wound infection, prolonged hospital stay, and increased medical cost [4–7]. Therefore, repair the dural defect and stop the leak of cerebrospinal fluid are difficult problems in clinical practice. Since the dura is a non-regenerative tissue [8], repair techniques or materials that can quickly seal leaks and promote the formation of surrounding fibrous connective tissue to close the dural defect are urgently needed. So far, many techniques and materials have been reported to repair spinal dural defect, including simple sutures, sealants, bioabsorbable staples, and various types of grafts and patches [9–14]. Among these repair methods, sutures will lead to needle holes leakage, and sealants can not meet the demand of dural defect repair because of its poor sealing effect in large spinal dural defect [15]. Different from the above repair method, the spinal patch has better physical properties and thinner thickness, and can be directly covered onto the surface of the dura mater to prevent the CSFL. However, the reported patches mostly require combination use of sutures or sealants to repair dural defect, and faces the problem of needle holes leakage and loose seal effect as well [16]. Therefore, it is urgent to develop a patch that can self-adhesive in wet environment and promote the formation of fibrous connective tissue

Abbreviations: CSFL, cerebrospinal fluid leakage; MBAA, N,N′-Methylene bisacrylamide; APS, ammonium persulfate; TEMED, N,N,N′,N′-Tetramethylethylenediamine; PBS, phosphate buffered saline; NHS, N-Hydroxysuccinimide; EDC, 1-(3-Dimethylaminopropyl)-3-ethylcarbodiimide hydrochloride; SEM, scanning electron microscope; CCK-8, cell counting kit-8; IHC, immunohistochemistry.

Peer review under responsibility of KeAi Communications Co., Ltd.

* Corresponding author.
E-mail address: zhaoyupumch@163.com (Y. Zhao).

[1] These authors contributed equally to this work.

https://doi.org/10.1016/j.bioactmat.2022.01.043
Received 20 November 2021; Received in revised form 13 January 2022; Accepted 24 January 2022
Available online 1 February 2022

to seal the dural defect. Unfortunately, there are no reports about self-adhesive patch to repair the spinal dura until now.

Recently, many researchers focused on the hydrogel for wound healing because of its excellent adhesion ability in wet environments [17]. However, the solidification of hydrogel usually needs the help of external methods such as light and heat. J. Mooney et al. reported an adhesive hydrogel that can bond to biological tissue by gently pressing in wet environments [18]. We propose that a wet high-viscosity hydrogel can achieved the sealing effect for the dural defect repair by little pressure rather than UV light or heating, which can not only avoid the pinhole leakage of suture and the limitation of sealant area in repairing the dual defect, but also can adjust the patch size according to the shape of the defect site.

In this work, a bioactive hydrogel patch for spinal dural repair was proposed, which consist of a chitosan adhesive and an alginate/polyacrylamide hydrogel dissipative matrix. This bioactive patch have excellent sealing function with the tolerance pressure was 790 ± 115.76 mmH_2O far exceeding the 200 mmH_2O physiological cerebrospinal fluid pressure. Furthermore, it was found that the patch could dramatically decrease the bacterial activity up to 99% after directly contacted for 48 h. Moreover, the bioactive patch can significantly enhance the fibroblasts proliferation promoting the formation of protective fibrous connective tissue, and also has the capabilities of anti-inflammatory and analgesic in the early postoperative period of spinal dural repair. This work shows great progress not only for the self-adhesive hydrogel's applications in spinal dural repair but also for clinical therapy of cerebrospinal fluid leakage and spinal dural defect sealing.

2. Methods

2.1. Preparation of the patch matrix

The following reagents were purchased from Sigma-Aldrich, unless otherwise noted. The patch consists of two parts, matrix and adhesive. The matrix was prepared by a two-step method. In the 1st step, 12% (w/v) acrylamide, 0.015 M calcium sulfate, 1% (w/v) sodium alginate (200 ± 20 mPa s) and 1% (w/v) low viscosity sodium alginate (3–5 mPa s) were dissolved in HBSS and stirred overnight to obtain a clear liquid. Add 360 μL 2% MBAA, 2260 μL 0.27 M APS, 80 μL TEMED to each 100 mL of the liquid. Pour the liquid into a 30 × 50 × 1/2/4 mm acrylic mold overnight. In the 2nd step, solidified hydrogel was taken out and immersed in the aqueous solution containing 0, 0.25 M, 0.50 M, 0.75 M and 1.00 M calcium chloride. After 24 h, the hydrogel was taken out and the surface liquid was removed before use. The hydrogel matrix with different water content were immersed in 0.25 M calcium chloride for 24 h, and the water content was reduced by volatilization at room temperature. Water content was determined by weighing before and after freeze-drying. The matrix used for physical property tests and animal experiments *in vivo* was 2 mm thick.

2.2. Preparation of the patch adhesive

Dissolve 0.2 g chitosan (low molecular weight), 0.12 g NHS, 0.12 g EDC in 10 mL MES buffer (pH 6.0). Before use, pour the adhesive onto the surface of hydrogel (5 μL per 1 mm^2) and press for 10 min.

2.3. Properties test of the patch matrix

2.3.1. Structured observation

After the patch matrix was freeze-dried, the surface and cross-sectional structure were observed under SEM (HITACHI UHR FE-SEM SU8020, Japan).

2.3.2. Tensile experiments

After measuring the length (L), width (W) and thickness (D) of the hydrogel, the patch matrix was fixed on both ends of the tensile testing machine (MarK-10, USA), and the tensile (F) and displacement (S) data were recorded at a speed of 50 mm/min to measure the maximum tensile stress and maximum tensile strain of the matrix. Young's modulus of the matrix was calculated.

$$\text{Stress} = F / (W \cdot D)$$

$$\text{Strain} = S / L \times 100\%$$

$$\text{Young's modulus} = (F \cdot L) / (W \cdot D \cdot \Delta L)$$

2.3.3. Swelling experiment

The patch matrix was soaked in PBS solution and measured for length, width, thickness and weight at 0, 1, 3, 5, 9, 24, 48, 72, 96, 120, 144, 168, 240 h.

2.4. Adhesion properties test of the patch adhesive

2.4.1. Adhesive experiments

Apply one patch to another patch matrix in contact with the adhesive layer and press them at 50 kPa for 5 min, the length (L) and width (W) of the bonded part of the patch were measured, fixed on both ends of the tensile testing machine (Mark-10, USA), stretched at a speed of 50 mm/min, and the tensile (F) and displacement (S) were recorded. The maximum adhesive force and the maximum tensile distance of the patch were measured.

$$\text{Adhesion} = F / W$$

2.4.2. The antibacterial experiment

The adhesive prepared as described above was poured into a mold and dried at 60 °C to form thin adhesive sheets. The sheets were cut into 1 cm discs and both sides were irradiated with UV for 30 min before use. The *Staphylococcus aureus* and *E. coli* were cultured in LB liquid medium at 120 r/min and 37 °C for 6 h. After the bacteria were diluted to 10^5 CFU/mL with PBS buffer, 1 disc adhesive sheet was added into 5 mL bacteria solution in the experimental group, and no substance was added into bacteria solution in the control group. Both groups were incubated at 120 r/min and 37 °C for 48 h, then diluted to the optimal concentration and inoculated on LB medium. Colony count was performed at 37 °C for 24 h.

2.5. In vitro cellular study

2.5.1. Cell experiment

Preparation of patch extract of each component.

DMEM used to prepare the extract were supplemented with 10% fetal bovine serum (FBS, Gibco, Grand Island, USA), 100 U/mL penicillin, and 100 mg/mL streptomycin (Gibco, Grand Island, USA).

Blank control: DMEM medium was placed at 4 °C for 24 h.

Matrix extract: Each 1 mL DMEM medium was added with 12 mg matrix, placed at 4 °C for 24 h, then removed and filtered with a 0.2 μm filter.

Adhesive extract: Add 2 μl adhesive to each 1 mL DMEM medium, place in 4 °C for 24 h, then filter with 0.2 μm filter.

Complex extract: Add 12 mg matrix and 2 μl adhesive to each 1 mL DMEM medium, place at 4 °C for 24 h, take out matrix, and filter with 0.2 μm filter.

2.5.2. Live/dead cell staining

L929 cells (Shanghai Jining Industrial Co., Ltd.) were inoculated in 96-well plates. The medium was changed into extract and cultured in an incubator at 37 °C with 5% CO_2 concentration for 1, 2, 3 days. Cells were stained with the Live/Dead™ Cell Imaging Kit (Thermo Fisher, USA),

photographed with a confocal microscope, and counted in ImageJ.

Living cell ratio = (number of living cells / total number of cells) × 100%

2.5.3. CCK-8 test

The cytotoxicity of the patch was tested using L929 cells (Shanghai Jining Industrial Co., Ltd.) and cell counting kit-8 (CCK-8, Dojindo, Japan). L929 were inoculated in 96-well plates and incubated in different extract at 37 °C in humidified atmosphere with 5% CO_2 concentration for 1, 2, 3 days.

Viability = (OD_{sample} -OD_{blank}) / ($OD_{control}$ -OD_{blank}) × 100%

2.6. Sealing test of patch

Fresh porcine small intestines and spines were purchased from abattoirs.

2.6.1. The maximum pressure test

The 5 mm catheter was ligated at both ends of the small intestine with sutures. After verifying that the small intestine is watertight, a 7 mm incision is made along the axial direction with a blade. The repair was performed by simple suture, fascial suture, patch paste and biological patch suture (made by bovine pericardium). A pressure sensor is attached to one end of the catheter and hydrostatic pressure is added to the other end to measure the pressure at the beginning of leakage from the incision. The suture group used 7-0 suture line for 7 stitches. In the fascia group, porcine autogenous fascia was packed on the defect site and interrupted suture using 7-0 suture line was performed for 7 stitches. In the biological patch group, the biological patch was covered on the defect and then interrupted suture using 7-0 suture line was performed for 7 stitches. In the patch group, the side of the patch adhesive was directly attached to the defect site of the small intestine, and apply 50 kPa pressure to the patch in the area where the patch meets the spinal dura with two acrylic plates for 5 min. The patch size is 25 × 15 mm.

2.6.2. Long time plugging test in wet environment

After the vertebral plates of the porcine spine were removed, a catheter was inserted and fixed between the two adjacent nerve root outlets. The peristaltic pump (LEAD-FLUID BF-100F, China) is used to transport the artificial cerebrospinal fluid with crystal violet added at a speed of 0.2 mL/min (consistent with the average flow rate of cerebrospinal fluid), and the other end of the catheter is connected to the waste liquid cylinder. A catheter was used above the dural defect to continuously drip artificial cerebrospinal fluid at a rate of 0.2 mL/min. Spinal dural defect and repair were performed as similar with that of the porcine small intestine model. The defect length was 3 mm, and the patch size was 3 × 5 mm. When the patch was attached, apply 50 kPa pressure to the patch in the area where the patch meets the spinal dura with both ends of blunt-ended forceps and lasted for 5 min. The area around the incision was covered with gauze soaked in saline. The spinal dural incision was photographed continuously by a camera.

2.7. In vivo effect test of patch

2.7.1. Animal experiment

The experiment was carried out using 8-week-old male SD rats. This was approved by the ethics committee of the Peking Union Medical Hospital (XHDW-2021-062). In brief, after anesthesia by intraperitoneal injection of pentobarbital sodium, a posterior median incision was made in the prone position, exposing the T9 to T11 thoracic vertebra. After the spinous process and lamina of the T10 thoracic vertebra were removed. The spinal dura mater was punctured with a needle to create a hole, and then lengthened axially by scissors to create a 3 mm defect. The defect was treated without treatment, fascial filling, patch sticking and biological patch (made by bovine pericardium) filling. The muscle and skin were then sutured layer by layer. The incision was closed directly in the untreated group. In the fascia group, 2 × 4 mm autogenous fascia was used to fill the defect site and then the incision was closed. In the biological mesh group, 2 × 4 mm biological patch was used to cover the defect site and then the incision was closed. The patch group was directly covered with 2 × 4 mm patch with adhesive side down, and the incision was closed after 5 min of compression at 50 kPa pressure in the area where the patch meets the spinal dura with two acrylic plates using both ends of blunt-ended forceps.

2.7.2. Immunohistochemistry (IHC) analysis

The spine from all groups were fixed in 10% neutral buffered formalin (NBF) solution for 48 h and then decalcified with 14% EDTA (pH 7.4) for 28 days. The samples were subsequently embedded in paraffin and cut into 5 μm sections. IHC was performed to detect inflammation around the defect and nerve damage in the spinal cord (1/2/3 weeks post-surgery). Histological slides were incubated with citrate buffer at 60 °C for heat-induced epitope retrieval and blocked with 1% hydrogen peroxide/methanol for 30 min at room temperature. Subsequently, they were incubated overnight at 4 °C with primary antibodies GFAP, Iba-1, MBP, TNF-α, and COX-2 (Servicebio, China). The color reaction was developed with ready-to-use 3,3′-diaminobenzidine color solution. The slides were counterstained with hematoxylin and visualized by a light microscope.

2.8. Statistical analysis

Graphpad Prism 8.0.2 (La Jolla, USA) was used to analyze the experimental data and the results were presented as the mean ± standard deviation (SD). Comparison between the 2 sets of data was performed using Student's *t*-test, and differences between the 3 or more groups of data were compared by one-way ANOVA. A value of $p < 0.05$ were considered to be statistically significant findings.

3. Result and discussion

3.1. Structure of the patch matrix

In this study, we fabricated a patch matrix consisting of polyacrylamide and sodium alginate (Fig. 1A) which can solidify in 5 min (Fig. 1B). Good transparency can be observed in freshly prepared hydrogels, and the transparency is increased after soaking in water while decreased after secondary cross-linking with calcium ions (Fig. 1C). The surface and interior of the matrix are porous structure observed by SEM (Fig. 1D). The pores of hydrogel without secondary cross-linking were not connected and could not provide an environment for the migration and growth of fibroblasts. After soaking in different concentrations of calcium ions for 24 h, the porosity and pore size of the patch matrix are improved obviously. Loose and porous matrix provides a suitable space for the growth and reproduction of fibroblasts, which is beneficial to the sealing of dural defects. The pore wall of the matrix soaked with 0 M calcium ions is weak and the strength is insufficient. The higher the concentration of calcium ions in the solution, the lower the connectivity of the pores, which inhibit the proliferation of fibroblasts. The 0.25 M calcium ions cross-linking group showed the best balance between pore wall thickness and pore connectivity. Furthermore, the surface cracks appeared with the increasing of calcium ions, we can see the cracks structure in the 0.5 M and 0.75 M calcium ions cross-linking groups. This may be due to calcium cross-linking agent increasing the stiffness of hydrogel while decreasing the toughness. The 0.25 M calcium ions cross-linking group may be the most suitable matrix because of its combination of toughness, stiffness, suitable porosity and pore size. The

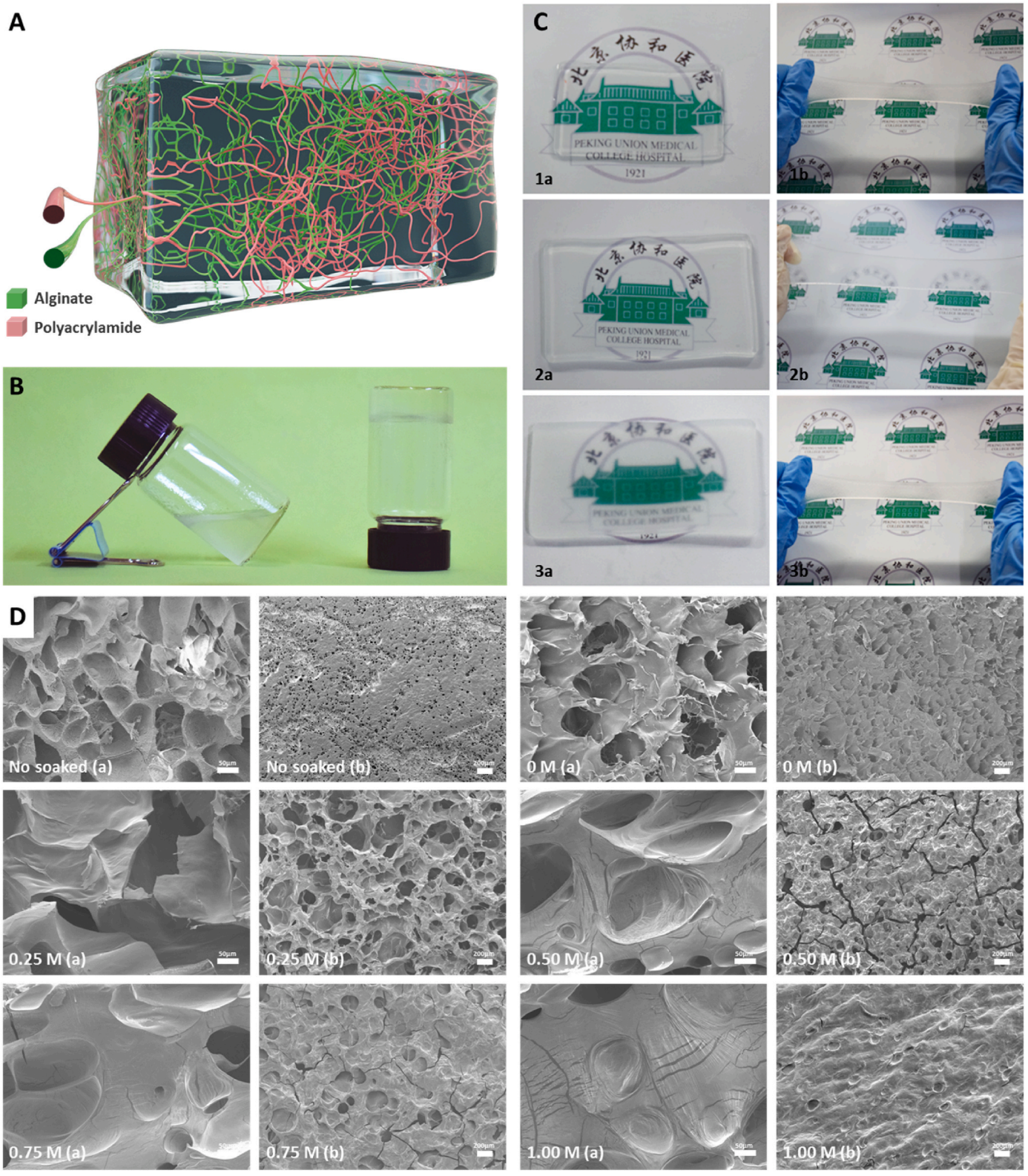

Fig. 1. The macroscopic and microscopic structure of patch matrix. (A) Schematic diagram of cross-linking structure of patch matrix. Green: Sodium alginate. Red: polyacrylamide. (B) Images of the patch matrix before (left) and after (right) coagulation. (C) Photographs of the patch matrix standing and stretching. 1: Patch matrix just removed from the mold. 2: Patch matrix soaked in water for 24 h 3. Patch matrix soaked in 0.25 M calcium chloride for 24 h. a: Stand. b: Stretched. (D) SEM photos of patch matrix soaked in different concentrations of calcium chloride No soaked: Patch matrix just removed from the mold. 0/0.25/0.50/0.75/1.00 M: Patch matrix soaked in 0/0.25/0.50/0.75/1.00 M calcium chloride for 24 h. a: cross section. b: surface.

appropriate porosity and pore size provide the comfortable environment for fibroblasts growth.

3.2. Tensile, swelling and adhesion properties of patch matrix

Most current patch systems are applied to the dura mater in the brain rather than that in the spine [19,20]. And most dural repair materials are sealants rather than patches. When repairing dural defects with commercial patches, only the sealing properties of the patch are concerned rather than the mechanical and adhesive properties [21]. The mechanical properties of hydrogel matrix are majorly determined by constituent ratio, water content, processing methods and so on [22]. The water content is a vital parameter to determine the mechanical property of the hydrogel. Aim to maximize the mechanical properties of the hydrogel matrix, we synthesized hydrogels with different water content (Fig. 2A), and cross-linked hydrogels with different concentrations of calcium ions, and tested the stretchability. The tensile strength and strain with different water content (all the matrix were soaked in 0.25 M calcium ion for 24 h and then dried naturally in the air to reduce water content) display linear correlation (Fig. 2B), in accordance with Hooke's law, indicating good elasticity of the hydrogels. The Young's modulus and breaking length of hydrogel matrix (the subscript means the water content) were calculated and summarized. The tensile stress, strain and Young's modulus of the matrix increase with the decreasing of water content. The 73% water content group showed the highest result in all groups. Its breaking strain reached 21.45 ± 1.84 times of the original length (Fig. 2C), with a tensile stress approached 149.41 ± 16.35 kPa (Fig. 2D) and Young's modulus was 22.29 ± 3.91 kPa (Fig. 2E). Whereas, in the practical application of patch and the matrix is in a highly hydrated state and the water content is much higher than 73%. Secondary crosslinking is a way to improve the tensile resistance of hydrogel. The crosslinking agent used in our patch is calcium ion, whose concentration will affect the tensile resistance of hydrogel matrix. Therefore, we tested the mechanical properties of hydrogel matrix

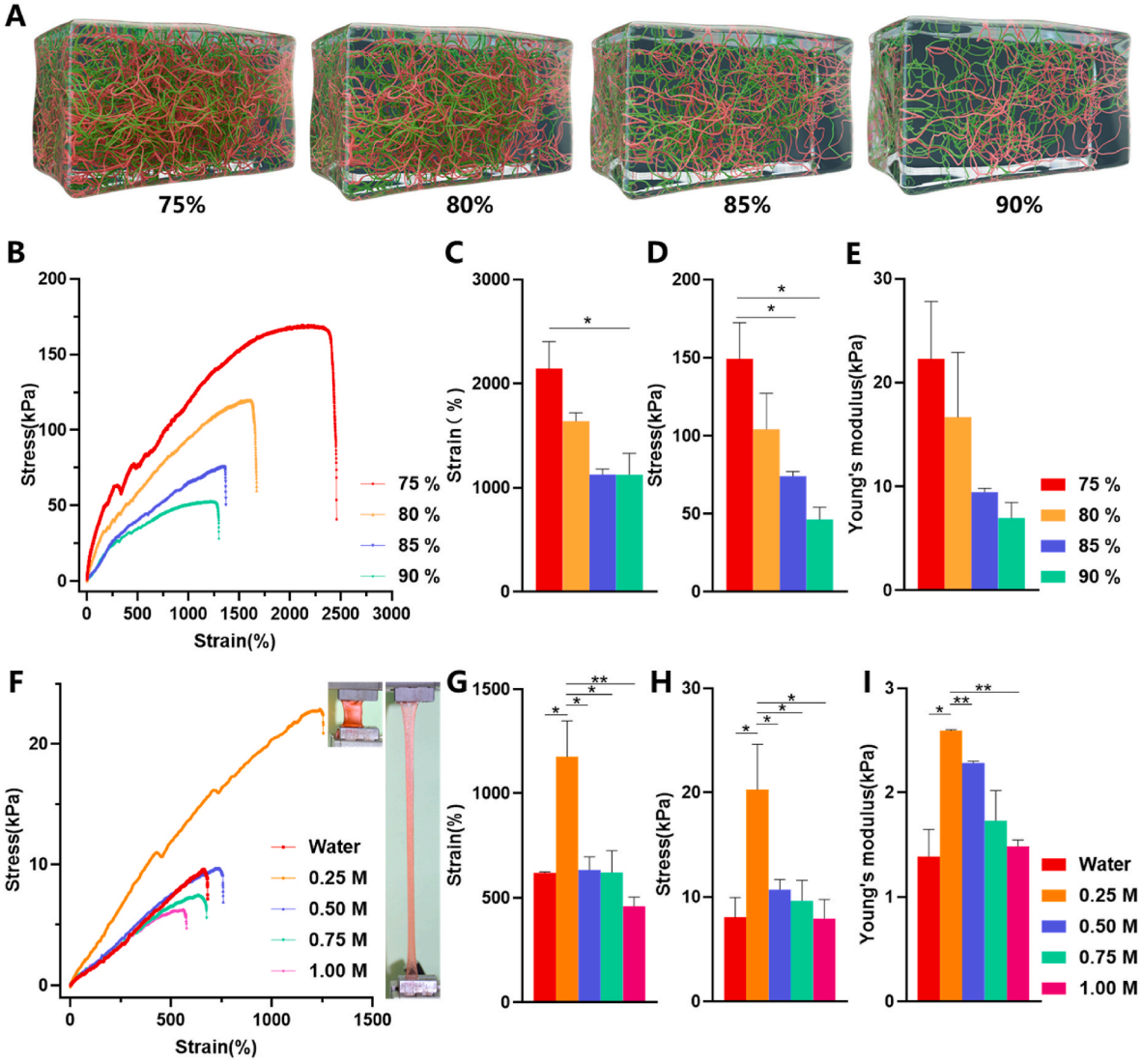

Fig. 2. The tensile properties of patch matrix soaked in different calcium concentrations and different water contents. (A) Schematic diagram of patch matrix with different water content. (B) Stress–strain curves of the hydrogel matrix with different water content. (C) The elongation at break (%) of patch matrix with different water content. (D) The tensile strength of patch matrix with different water content. (E) The Young's modulus of patch matrix with different water content. All the matrix used from (B) to (E) were soaked in 0.25 M calcium ion for 24 h and then dried naturally in the air to reduce water content. (F) Stress–strain curves of the hydrogel matrix soaked in different calcium concentrations for 24 h. The inset of (F) shows a sample with a dimension of 15 mm in length, 10 mm in width, and 2 mm in thickness without stretch (left) and while stretched to 800% (right). (G) The elongation at break (%) of patch matrix soaked in different calcium concentrations. (H) The tensile strength of patch matrix soaked in different calcium concentrations. (I) The Young's modulus of patch matrix soaked in different calcium concentrations. Data are presented as mean ± SD. *P < 0.05 and **P < 0.01, significant difference among different group.

soaked in calcium ion solution for 24 h, and identified the impact of secondary crosslinking with different concentrations of calcium ions on mechanical properties. The tensile strength and strain with different calcium ion secondary crosslinking display linear correlation (Fig. 2F) as well (the subscript means the concentrations of calcium ions). However, there is no linear relationship between the increase of crosslinker concentration and the tensile properties of hydrogel matrix. The toughness of the materials decreased after the secondary immersion with higher concentration of crosslinker (more than 0.25 M), which was consistent with the results observed by electron microscopy. The 0.25 M group showed the highest of all. The breaking strain was 11.76 ± 1.72 times of the original length (Fig. 2G), with a tensile stress reached 20.28 ± 4.34 kPa (Fig. 2H) and Young's modulus was 2.56 ± 0.01 kPa (Fig. 2I). The maximum stress of the spinal dura for the longitudinal direction is over 40 MPa and the breaking strain is 0.55 times, while the maximum stress for the circumferential is over 6 MPa and the breaking strain is 0.2 times [23,24]. The strain properties of our patch are much higher than the properties of the dura mater itself. In practice, the dura is only slightly bent, and the stress changes are within the range that our patch can withstand. Thus, the tensile properties of freshly prepared 0.25 M group hydrogel matrix (the calculated water content is more than 95%) fully meet the requirements of spinal cord and dural activity after spinal dural repair since spinal cord mobility *in vivo* is very low.

Due to the water absorption properties of hydrogel matrix, potential spinal cord compression problems may arise when used for dural defect repair. Hence, we prepared standard size hydrogels matrix (3 × 5 mm) with different thickness (without soaking in the calcium ion for secondary crosslinking) using the mold and tested their swelling ratio by soaking in the PBS. The water absorption efficiency of the matrix is different according to its thickness. After 10 days, all matrix nearly reached saturated swelling level, and the weight swelling ratios were 5.34 ± 0.28 times, 5.83 ± 0.40 times, 6.13 ± 0.46 times (Fig. 3A) the original weight of 1 mm, 2 mm and 4 mm thick matrix respectively. And the volume swelling ratios after 10 days were 5.62 ± 0.27 times, 5.92 ± 0.35 times, 6.49 ± 0.33 times (Fig. 3B) the original volume of 1 mm, 2 mm and 4 mm thick matrix respectively.

After absorbing water, the weight and volume of the patch expand to about 6 times of the original, which may be a potential compression on the spinal cord. However, the spinal cord is located in an environment of cerebrospinal fluid, which is composed primarily of water. The dry

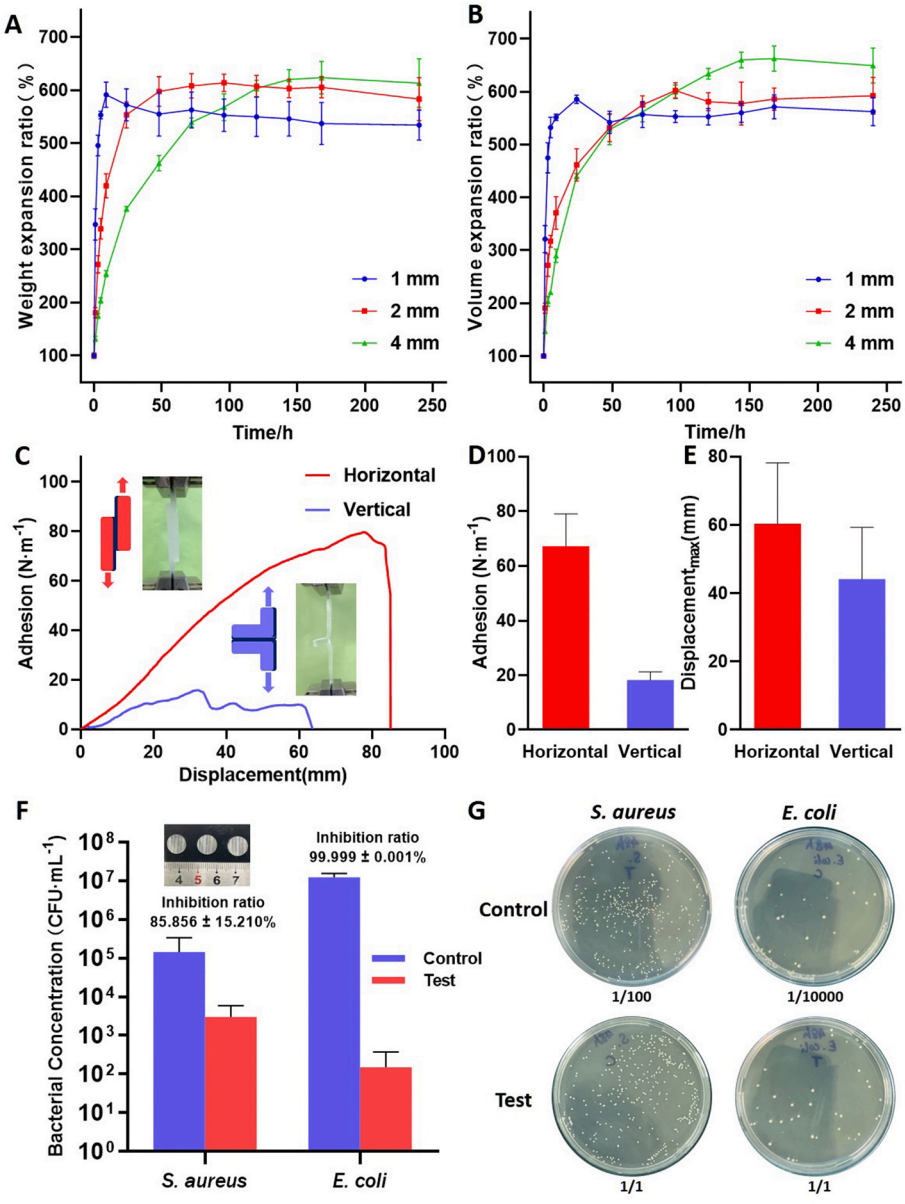

Fig. 3. The weight and volume change of the patch after absorbing water and the adhesion and antibacterial function of the adhesive. (A) The weight expansion ratio of patch matrix with size of 3 × 5 mm and thickness of 1 mm, 2 mm and 4 mm soaked in PBS. (B) The volume expansion ratio of patch matrix with size of 3 × 5 mm and thickness of 1 mm, 2 mm and 4 mm soaked in PBS. (C) Adhesion-displacement curves obtained by stretching two patches along the horizontal and vertical directions of the bonding surface. The insert diagrams and photos of (C) show the horizontal (left, red) and vertical (right, blue) directions mean the directions parallel and perpendicular to the bonding surface. (D) The maximum adhesion of the adhesive in two directions. (E) The maximum displacement of the adhesive in two directions. (F) Bacteriostatic effect of adhesive and bacteria after co-culture for 48 h. Control indicates that no adhesive is added to the bacterial solution. Test indicates that an adhesive has been added to the bacterial fluid. The inserted picture shows the dry adhesive layer. (G) Original image of colony count. (The number below each photo indicates dilution). Data are presented as mean ± SD. *P < 0.05 and **P < 0.01, significant difference among different group.).

weight of the patch itself is very low (0.43 ± 0.00067 g for a standard 3 × 5 × 2 mm patch matrix). The pressure caused by the patch on the spinal cord is relatively small in theory because the main weight of patch comes from water. The thickness of the saturated matrix is less than twice that of the original, and the compression effect on the spinal cord is insignificant. We observed that after soaking for 24 h, the weight swelling ratio of 1 mm, 2 mm and 4 mm thick matrix account for 107.57 ± 7.72%, 95.12 ± 3.18% and 61.59 ± 2.80% of 10 days' weight swelling ratio respectively. And the volume swelling ratio of 1 mm, 2 mm and 4 mm thick matrix is 104.26 ± 2.85%, 77.89 ± 0.38% and 67.89 ± 1.96% of that of 10 days respectively. Since the calcium ion secondary crosslinking method that we used requires reacted for 24 h, and the 1 mm and 2 mm matrices have nearly reached saturation swelling after soaking for 24 h, we selected the matrix with 2 mm and 1 mm initial thickness after soaking in calcium ions for 24 h in the subsequent *in vitro* experiments and *in vivo* experiments.

After demonstrated the excellent mechanical properties of the hydrogel matrix, we further investigated the adhesive capacity of the chitosan adhesive. We chose the matrix soaked in 0.25 M calcium ions for 24 h for all subsequent experiments in view of its suitable pore structure and best tensile properties. After the two matrices are bonded by chitosan adhesive, the adhesive force and displacement showed a linear relationship in the direction parallel to the bonding surface (horizontal direction indicated in the figure), and a nonlinear relationship in the direction perpendicular to the bonding surface (vertical direction indicated in the figure) (Fig. 3C). The adhesive force in the horizontal direction was 67.24 ± 11.86 N m^{-1} and that in the vertical direction was 18.27 ± 3.00 N m^{-1} (Fig. 3D). The maximum tear resistance distance is 60.38 ± 17.78 mm in horizontal direction and 44.10 ± 15.13 mm in vertical direction (Fig. 3E). The tearing force that patch faces in practical application is mainly from horizontal friction. The patch position is relatively stable after the wound is closed during surgery, and the current adhesion property can meet the practical requirements. In addition to the above studies, failure to repair spinal dural defects due to patch degradation must be considered in the repair process. However, the degradation performance of similar alginate/polyacrylamide hydrogel network system is rarely reported, and the latest derivative system showed a weight loss of less than 30% within 8 weeks [25]. The long-term degradation performance of the patch also needs to be further studied. In summary, the 0.25 M group patch matrix combined with chitosan adhesive can maintain good adhesion effect in the dural defect environment, avoid the failure of sealing caused by needle holes leakage and unstable adhesion.

3.3. Antimicrobial test of adhesive

Infection after dural injury and material implantation are the most common complications of spinal surgery [6,26]. Chitosan can form a complex with the cell membrane or interfere with gene expression, inhibiting the uptake of trace elements and nutrients that are necessary for bacterial growth, to achieve an antibacterial effect [27,28]. And our adhesive is chitosan crosslinked in MES buffer with the assistance of NHS and EDC. In order to explore the potential antibacterial effect of the adhesive, adhesive discs with a diameter of 1 cm were prepared and cultured directly with *S. aureus* and *E. coli* for 48 h in test group. Bacterial concentrations were determined by colony counting. The concentration of *S. aureus* and *E. coli* decreased by 85.956 ± 15.210% and 99.999 ± 0.001% in 48 h, respectively (Fig. 3F). Fig. 3G showed photos of the bacteria colony after 48 h with or without the adhesive. The number at the bottom of the photo represents the dilution ratio of bacterial solution before coating plate. The test group must observe the appropriate number of bacterial colonies under the condition of coating plate without dilution, and the control group needed to dilute 1/100 or 1/10000. The adhesive showed excellent antibacterial effect, especially against Gram-negative bacteria like *E. coli*. The incidence of postoperative infection can be decreased through the antibacterial properties of patch itself, which has important biological significance to prevent postoperative complications.

3.4. Sealing effect in wet environment

To study the short-term and long-term sealing effect of the patch in the wet environment, we constructed two *in vitro* models of porcine small intestine and porcine spinal cord to simulate the status of the patch in repairing dural defect. The experimental model used to test the maximum liquid pressure that the patch could withstand in a short period was mainly composed of an infusion bag, porcine small intestine and the sensor (Fig. 4A). The pressure on the defect was increased by increasing the height of the liquid level and the sensor recorded the instantaneous pressure at which fluid leakage occurred at the defect repaired site. After making a 7 mm incision along the axis of the small intestine, our bioactive patch, suture, fascia, and biological patch were used for repair respectively. Instant coating adhesive is adopted in our experiment. However, the preparation of pre-coated products is feasible. If pre-coated patch is to be carried out, irradiation sterilization is recommended. But the effect of irradiation on matrix strength needs further experimental verification. Considering that the patch contains a lot of water, medical propylene polymer material is suggested to use for the outer packaging of the patch. 50 kPa pressure for 5 min with the adhesive side toward the defect was the only need for our patch, compared with other repair methods which need to use suture lines for meticulous and intensive intermittent suture. Even so, the patch can withstand pressure of 790 ± 115.76 mmH_2O (Fig. 4B), well above the upper limit of other repairing methods including direct suture, post-fascial packing suture, biological patch suture and reports in other commercial sealants or patches that just less than 300 mmH_2O [14,21]. The key and most important issue of dural repair is its sealing performance, in other words, its ability to resist the pressure of cerebrospinal fluid under physiological or pathological conditions. Normal cerebrospinal fluid pressure does not exceed 200 mmH_2O, and even under pathological conditions it does not exceed 600 mmH_2O, which is lower than the maximum pressure that the patch can bear under the premise of ensuring the sealing effect. The deformation ability and high water's content of hydrogel matrix dispersed the pressure at the defect site, thus achieving a good sealing effect under the condition of not high adhesion force. The sealing ability of the patch in unilateral fluid environment can meet the needs of dural defect repair.

In order to visually observe the long-term changes of the patch in repairing spinal dural defects, an *in vitro* model consisting of an infusion bag, a peristaltic pump, a porcine spine and catheters were constructed (Fig. 4C). The flow speed of physiological cerebrospinal fluid (0.2 mL/min) was simulated through a peristaltic pump. Wet gauze and continuous drops of artificial cerebrospinal fluid were used to simulate the wet environment inside the body. To detect leakage in the defect, crystal violet was added to the artificial cerebrospinal fluid to visualize it. The lamina of each experiment level was removed and two catheters used to circulate artificial cerebrospinal fluid was fixed at both ends of the level with knots (Fig. 4D). No leakage of artificial cerebrospinal fluid from the patch was observed after 72 h (Fig. 4E) of continuous filming in wet environment. The patch still maintained a good sealing effect after a long-time infiltration with artificial cerebrospinal fluid which had simulated the calcium concentration of cerebrospinal fluid, indicating that the effect of physiological calcium ions around the patch was not enough to cause the repair failure. The experiment was aborted due to ventral dural damage caused by spinal cord decay after 3 days. However, it was preliminarily confirmed that the patch could maintain a good sealing effect in the wet environment of real dural defects.

3.5. In vitro cellular study

Before applying the patch in animals, we tested the biocompatibility of each component of the patch and its overall *in vitro*. Live and dead cell

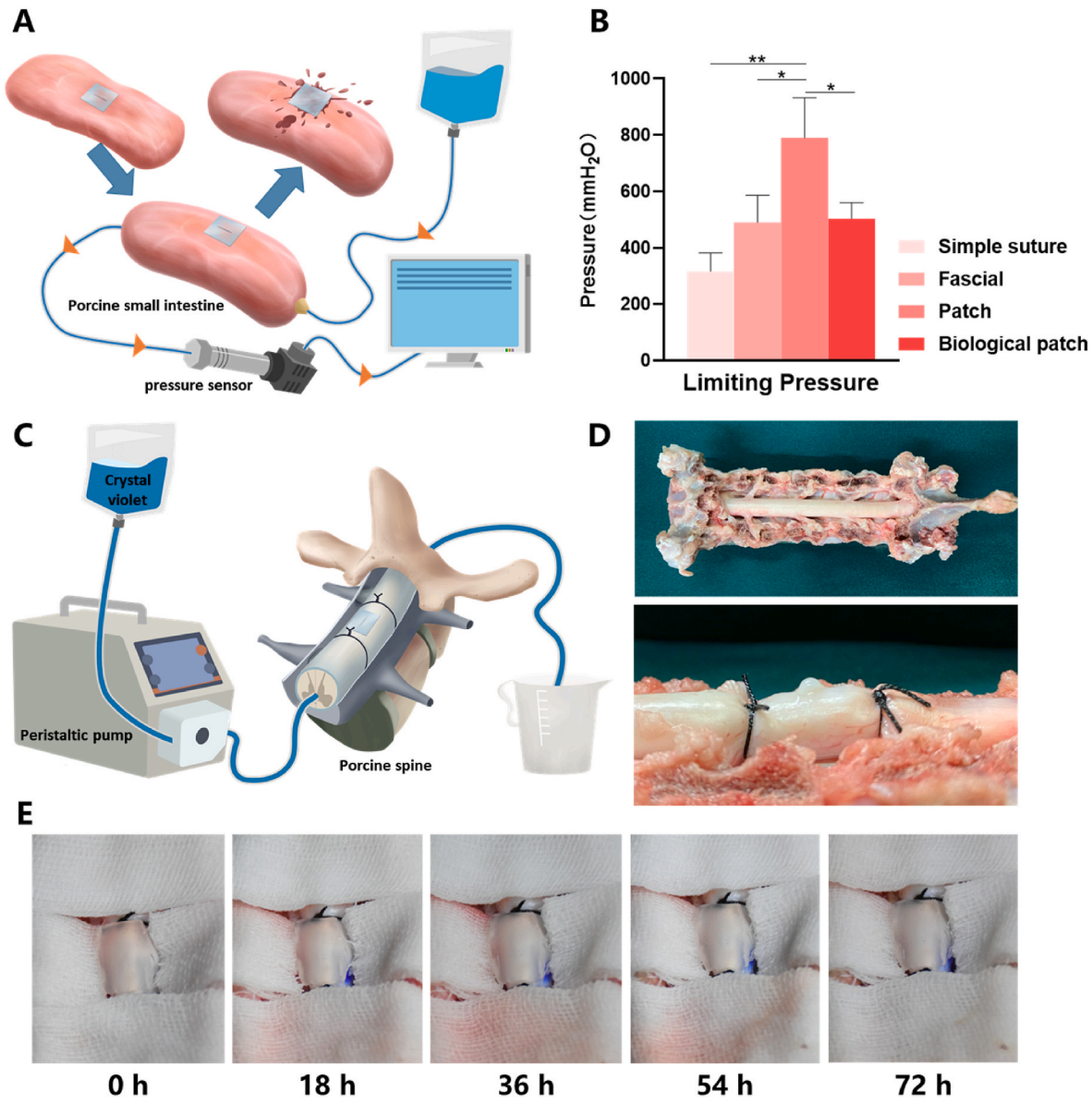

Fig. 4. The results of the sealing effect of different spinal dural defect repair methods. (A) Schematic diagram of limit pressure test of spinal dural defect repair methods using porcine small intestine. (B) Limit pressure of different spinal dural defect repair methods. (C) Schematic diagram of experimental model of spinal dural defect repair by patch in porcine spinal dura. (D) Pictures of the porcine spinal cords used in the experiment. (E) Photos of the spine at different times after dural defects were repaired using patches. Data are presented as mean ± SD. *P < 0.05 and **P < 0.01, significant difference among different group.

staining and CCK-8 were used to define the effects of patch on the survival and proliferation of L929 cells, respectively., and selected 0.25 M group for live and death staining. The matrix, the adhesive, and the complete patch are not shown obvious cell death in the staining of live dead cells (Fig. 5A). There was no significant difference in the ratio of living cells between each group and the negative control group at day 1, 2 and 3 (Fig. 5B) by counting the staining results of living and dead cells. While in CCK-8 experiment, we used the extracts liquid of the patch to explore the cell proliferation promoting potential of complete patch, adhesive and hydrogel matrix with secondary cross-linking using different calcium ions (Fig. 5C). Except for the matrix soaked with 0 M calcium ion at day 1($P < 0.05$), the cell viability of the matrix, adhesive and patch soaked with different concentrations of calcium ion showed no significant decrease at day 1, 2 and 3. The matrix soaked with 0.25 M calcium ion showed a significant increase in cell viability on the first day ($P < 0.01$). Combined with the results of SEM, the fibroblasts on the 0.25 M patch group not only had the most suitable structure for fibroblast growth, but also had the best potential to promote cell proliferation, which was conducive to the early repair of dural defect. The matrix group underwent 0.25 M calcium ion secondary cross-linking showed good biocompatibility and potential early promotion of fibrocyte proliferation in cell experiments, which also have the best mechanical properties as previously indicated. Hence, we chose it as the patch matrix for our application *in vivo* in the following animal experiments. Although the cell experiments have fully demonstrated that the material does not cause adverse effects on cell proliferation and survival, the residual monomers (acrylamide, MBAA, EDCA and NHS) should be analyzed to reduce the cytotoxicity. More quantitative residual monomer tests are needed before the patch can be commercialized.

3.6. *Biological function in vivo*

To study the biological effects of our mesh *in vivo*. SD rats were anesthetized by pentobarbital sodium and the surgical site was exposed

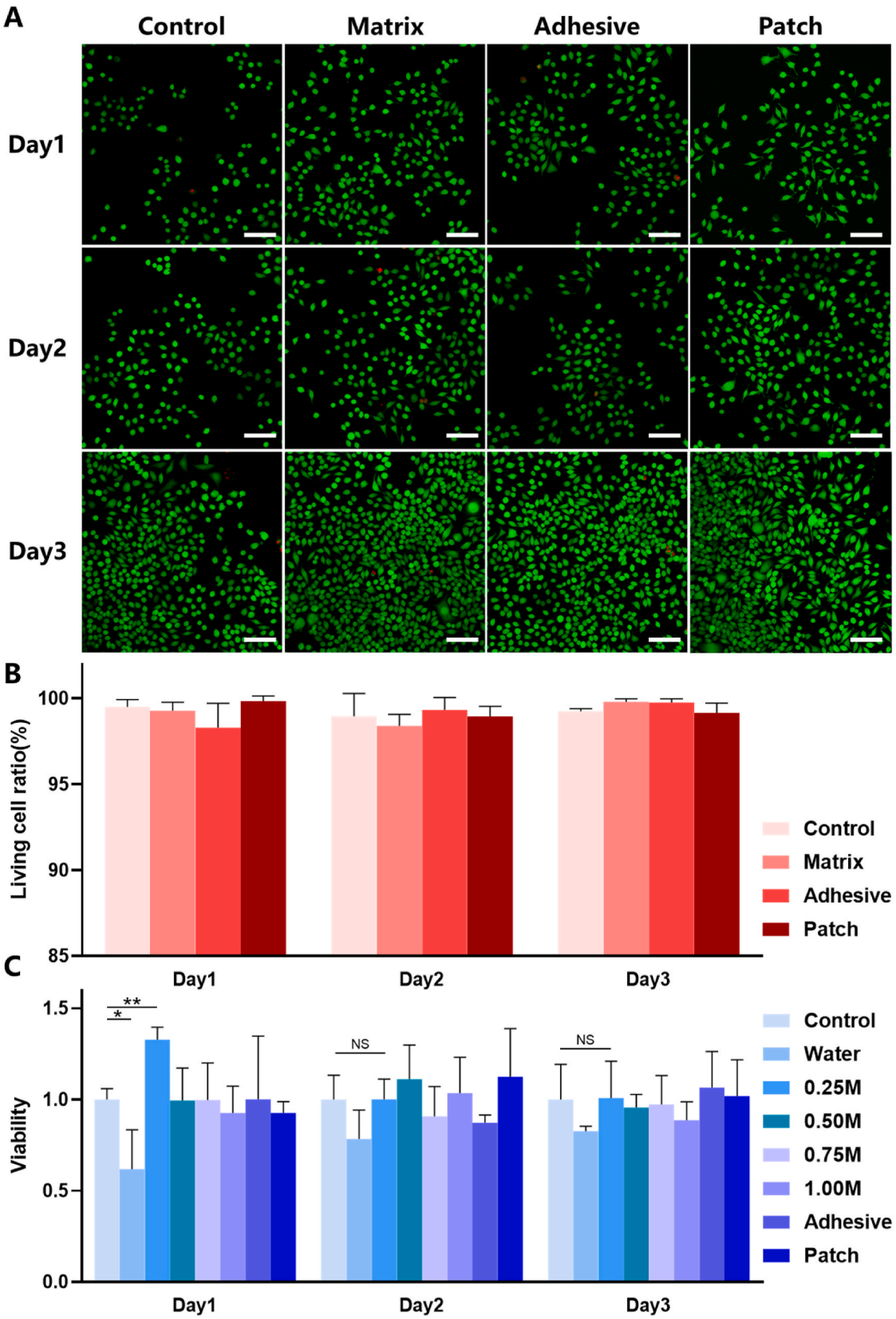

Fig. 5. Effect of patch on proliferation and survival of L929 cells. (A) Live/dead cells staining images of L929 cells cultured with extracts of different components in patch. (B) CCK-8 results of L929 cells cultured with extracts of different components in patch. (C) Living cell ratio of L929 cells cultured with extracts of different components in patch. Data are presented as mean ± SD. *P < 0.05 and **P < 0.01, significant difference among different group. The scale means 200 μm. NS: No significance.

layer by layer. The lamina was removed and 3 mm axial spinal dural defect was created by needle and scissors, then dural repair was performed in different ways. In the fascia repair group, autologous fascia was used for packing, and in the biological patch group, a patch from bovine pericardium was used for direct covering. For our patch, apply 50 kPa pressure for 5 min in the area where the patch meets the spinal dura with blunt-ended forceps was the only need (Fig. 6A). All the experimental animals survived well and showed regular behavior. There were no effusion, exudation and infection in the incision, rejection, epilepsy or other postoperative complications.

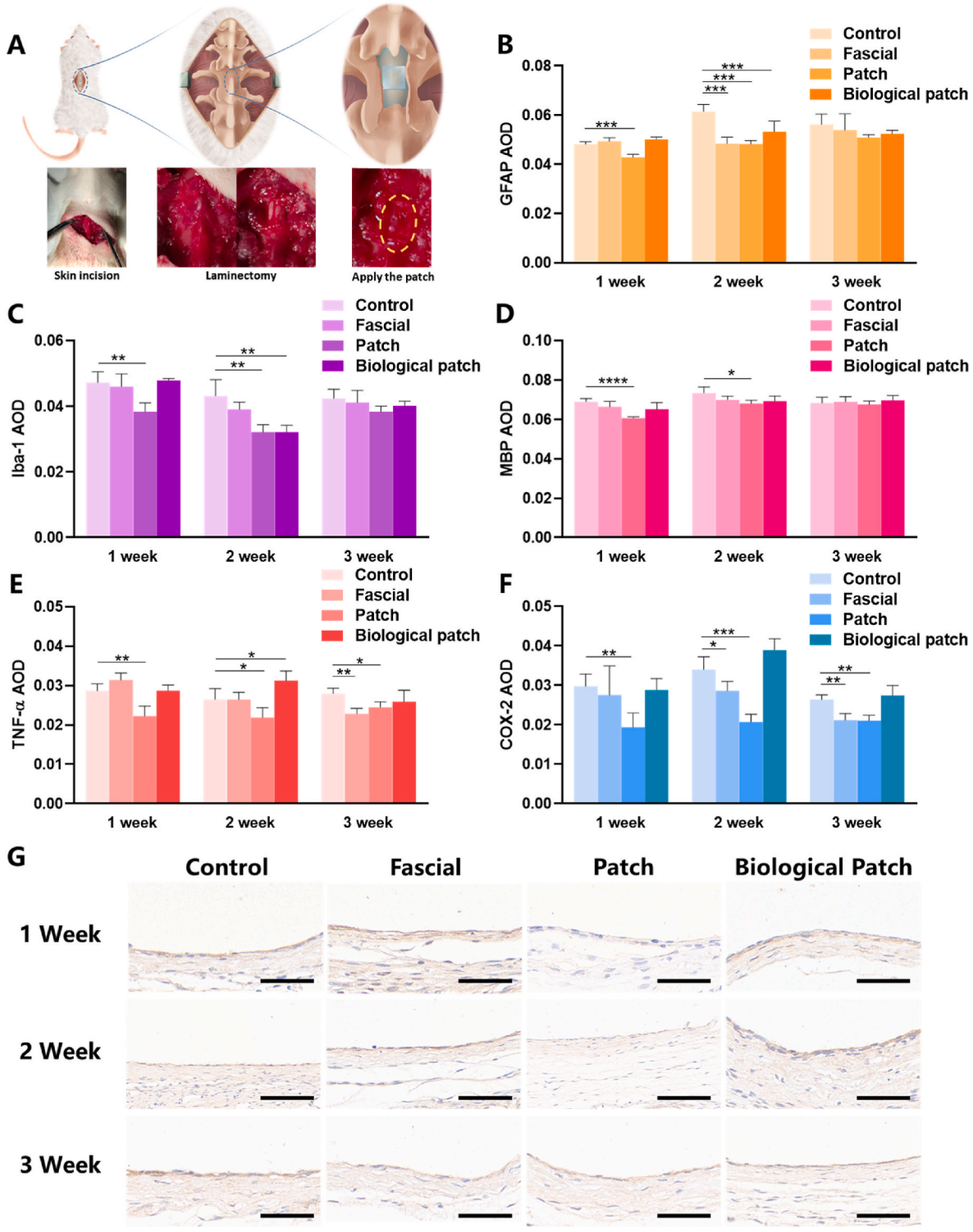

Fig. 6. Immunohistochemical results of different spinal dural repair methods. (A) Schematic diagram of animal model of spinal dural defect in rats. Surgical photos are inserted below the schematic. (B) AOD values of GFAP in the spinal cord. (C) AOD values of Iba-1 in the spinal cord. (D) AOD values of MBP in the spinal cord. (E) AOD values of TNF-α in the surrounding tissues of dural defects. (F) AOD values of COX-2 in the surrounding tissues of dural defects. (G) The images of rats' spinal dural after immunohistochemical staining (TNF-α). Data are presented as mean ± SD. *P < 0.05 and **P < 0.01, significant difference among different group. The scale means 50 μm.

Spinal dural defects can lead to pathological changes in the ventral spinal cord and surrounding dorsal tissues, including the formation of nerve scar caused by oligodendrocytes and astrocytes, the regulation of immune microenvironment by microglia and macrophages, and the regulation of inflammatory microenvironment by various inflammatory cells and inflammatory factors (such as TNF-α and COX, etc.) (Fig. 7).

After spinal dural injury, inflammation may occur around the injury site, mediating spinal cord demyelination and scar tissue formation [29]. MBP is present in the central nervous system and acts as a link between layers of myelin sheath around axons [30]. The increased reactivity of MBP after injury is associated with the "reactivity" of oligodendrocytes, which is associated with local scar repair [31]. The expression levels of MBP (Fig. 6D) in the spinal cord were significantly lower than those in the control group in the first week. This suggests the potential role of our bioactive patch in reducing nerve scarring. GFAP is specifically expressed in astrocytes and is closely associated with meningeal fibrosis and scarring at the site of injury [32–34] (Fig. 7). The expression levels of GFAP (Fig. 6B) in the first and second week were also significantly lower than those in the control group. This phenomenon once again highlights the potential role of our bioactive patch in reducing nerve scarring. The immune microenvironment is essential to ensure the normal repair of surrounding tissues after spinal dural injury. Microglia and macrophages are important components of immune microenvironment. Iba-1 is specifically expressed in microglia/macrophages and promotes cell migration and phagocytosis [35,36]. Reduced microglial activation provides a neuroprotective immune microenvironment [37]. The expression levels of IBA-1 (Fig. 6C) in the first and second week were also significantly lower than those in the control group. Although none of the rats developed neurological complications in the early postoperative period, spinal tissue around dural defects repaired with patch showed down-regulation of GFAP, IBA-1, and MBP in the early postoperative period (1–2 weeks), indicating that our patch may inhibit oligodendrocyte, astrocyte, and microglia/macrophage responses in early period, reduce connective tissue scarring, alleviate macrophage accumulation and progressive secondary injury by limiting meningeal fibrosis. More detailed biological pathways need to be explored with more time and experiments, using new tools such as single-cell sequencing in the future.

An inflammatory response can occur in any injury and can directly affect symptoms such as pain. Both TNF-α and COX-2 play important roles in inflammation, cell growth control, and pain-related neurotransmitter transmission [38,39]. TNF-α not only promoted the meningeal nociceptor mediated by COX activity and increased the dura pain response, but also directly acted on the TNF receptor of neuronal cells to promote the activation and sensitization of nociceptor [40]. TNF-α promotes the activation and sensitization of nociceptive receptors by directly acting on neuronal TNF receptors [41,42]. Down-regulation of COX mitigated the pain-promoting state produced by injury/inflammation and direct activation of glutamate and substance P receptors in the spinal cord [43] (Fig. 7). The expression of TNF-α and COX-2 (Fig. 6E and F) around the dural defect was significantly down-regulated in the 1/2/3 weeks compared with the control group, and the IHC images (Fig. 6G) showed significantly down-regulated expression of TNF-α. It's suggested that the patch may have biological effects of inhibiting inflammation and alleviating pain.

4. Conclusion

In summary, we developed a multifunctional bioactive patch to repair spinal dural and prevent CSFL occurs with excellent properties of tight sealing, anti-inflammatory, pain relieving and antibacterial. Additionally, the bioactive patch can promote fibroblasts cell proliferation through the formed porous structure, which could accelerate the sealing process of spine dural defect. In addition, it demonstrated that

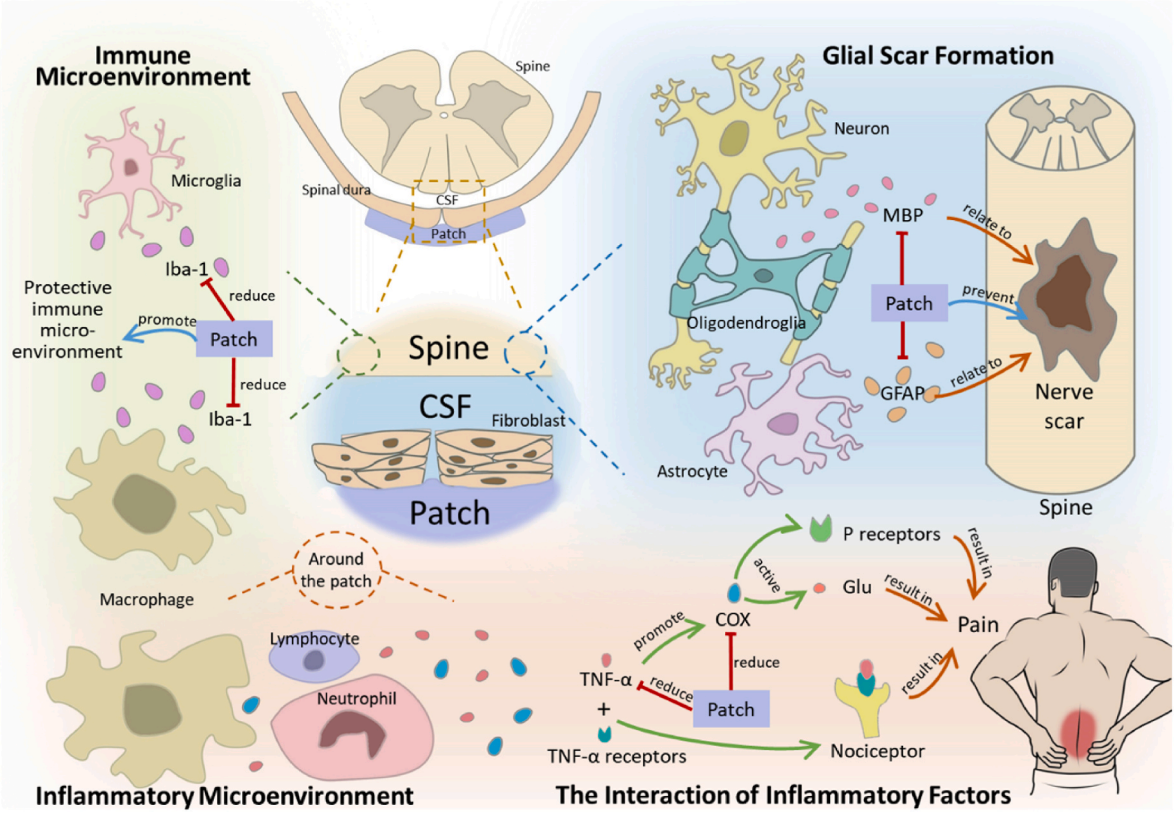

Fig. 7. Partial biological effects of patch repair on spinal dura. The dotted line indicates the enlargement of the local area. "Patch" means the bioactive patch that we study and manufacture. CSF: cerebrospinal fluid.

the adhesive layer of the patch showed excellent inhibition ability on *E. coli* and *S.aureus* with the sterilizing rate were 99.999% ± 0.001% and 85.956 ± 15.210%, which could significantly reduce the incidence of postoperative infection. Moreover, cytokines such as GFAP, IBA-1 and MBP associated with inflammation, pain, and scar formation were significantly down-regulated at 1–3 weeks postoperatively, enhancing the anti-inflammatory, analgesic, and antiadhesion effects around the defect site. Furthermore, easy availability and low cost make the bioactive patch a reliable choice for spinal dural defect repair in clinic.

CRediT authorship contribution statement

Jiahao Li: Conceptualization, Methodology, Formal analysis, Investigation, Visualization, Writing – original draft. **Jingjing Tian:** Conceptualization, Validation, Investigation, Writing – review & editing. **Chunxu Li:** Investigation. **Longyun Chen:** Investigation. **Yu Zhao:** Conceptualization, Supervision, Project administration.

Declaration of competing interest

All authors declare that they have no financial and personal relationships with other people or organizations that can inappropriately influence our work, there is no professional or other personal interest of any nature or kind in any product, service and/or company that could be construed as influencing the position presented in, or the review of, the manuscript entitled.

Acknowledgements

Jiahao Li and Jingjing Tian contribute equal to this work. Yu Zhao conceived, designed and supervised the study; Jiahao Li, Jingjing Tian, Chunxu Li, Longyun Chen conduct experiments and led the statistical analysis of the data; The first draft of the manuscript was written by Jiahao Li and Jingjing Tian. All authors read and approved the final manuscript before submission. This work was supported by Tsinghua University-Peking Union Medical College Hospital Initiative Scientific Research Program (20191080871) and the National Natural Science Foundation of China (82002314).

References

[1] S.J. Nagel, C.G. Reddy, L.A. Frizon, M.K. Chardon, M. Holland, A.G. Machado, G. T. Gillies, M.A. Howard 3rd, S. Wilson, Spinal dura mater: biophysical characteristics relevant to medical device development, J. Med. Eng. Technol. 42 (2) (2018) 128–139, https://doi.org/10.1080/03091902.2018.1435745.

[2] J.M. Oertel, B.W. Burkhardt, Full endoscopic treatment of dural tears in lumbar spine surgery, Eur. Spine J. 26 (10) (2017) 2496–2503, https://doi.org/10.1007/s00586-017-5105-8.

[3] G.M. Ghobrial, T. Theofanis, B.V. Darden, P. Arnold, M.G. Fehlings, J.S. Harrop, Unintended durotomy in lumbar degenerative spinal surgery: a 10-year systematic review of the literature, Neurosurg. Focus 39 (4) (2015) E8, https://doi.org/10.3171/2015.7.FOCUS15266.

[4] M.H. Khan, J. Rihn, G. Steele, R. Davis, W.F. Donaldson 3rd, J.D. Kang, J.Y. Lee, Postoperative management protocol for incidental dural tears during degenerative lumbar spine surgery: a review of 3,183 consecutive degenerative lumbar cases, Spine 31 (22) (2006) 2609–2613, https://doi.org/10.1097/01.brs.0000241066.55849.41.

[5] P. Guerin, A.B. El Fegoun, I. Obeid, O. Gille, L. Lelong, S. Luc, A. Bourghli, J. C. Cursolle, V. Pointillart, J.M. Vital, Incidental durotomy during spine surgery: incidence, management and complications. A retrospective review, Injury 43 (4) (2012) 397–401, https://doi.org/10.1016/j.injury.2010.12.014.

[6] C. Weber, J. Piek, D. Gunawan, Health care costs of incidental durotomies and postoperative cerebrospinal fluid leaks after elective spinal surgery, Eur. Spine J. 24 (9) (2015) 2065–2068, https://doi.org/10.1007/s00586-014-3504-7.

[7] M.J. Luszczyk, G.Y. Blaisdell, B.P. Wiater, C. Bellabarba, J.R. Chapman, J.A. Agel, R.J. Bransford, Traumatic dural tears: what do we know and are they a problem? Spine J. 14 (1) (2014) 49–56, https://doi.org/10.1016/j.spinee.2013.03.049.

[8] F. Qu, Q. Li, X. Wang, X. Cao, M.H. Zgonis, J.L. Esterhai, V.B. Shenoy, L. Han, R. L. Mauck, Maturation state and matrix microstructure regulate interstitial cell migration in dense connective tissues, Sci. Rep. 8 (1) (2018) 3295, https://doi.org/10.1038/s41598-018-21212-4.

[9] Y. Shimada, M. Hongo, N. Miyakoshi, T. Sugawara, Y. Kasukawa, S. Ando, Y. Ishikawa, E. Itoi, Dural substitute with polyglycolic acid mesh and fibrin glue for dural repair: technical note and preliminary results, J. Orthop. Sci. 11 (5) (2006) 454–458, https://doi.org/10.1007/s00776-006-1044-7.

[10] C.A. Bohoun, T. Goto, H. Morisako, A. Nagahama, Y. Tanoue, K. Ohata, Skull base dural repair using autologous fat as a dural substitute: an efficient technique, World Neurosurg. 127 (2019) e896–e900, https://doi.org/10.1016/j.wneu.2019.03.293.

[11] Y. Jing, X. Ma, C. Xu, H.L. Tian, S.W. Chen, Repair of dural defects with electrospun bacterial cellulose membranes in a rabbit experimental model, Mater. Sci.Eng. C Mater. Biol. Appl. 117 (2020) 111246, https://doi.org/10.1016/j.msec.2020.111246.

[12] A. Iwata, M. Takahata, K. Kadoya, H. Sudo, T. Kokabu, K. Yamada, N. Iwasaki, Effective repair of dural tear using bioabsorbable sheet with fibrin glue, Spine 42 (18) (2017) 1362–1366, https://doi.org/10.1097/BRS.0000000000002095.

[13] T. Zhu, H. Wang, Z. Jing, D. Fan, Z. Liu, X. Wang, Y. Tian, High efficacy of tetra-PEG hydrogel sealants for sutureless dural closure, Bioact. Mater. 8 (2022) 12–19, https://doi.org/10.1016/j.bioactmat.2021.06.022.

[14] W. Deng, Y. Tan, M.S. Riaz Rajoka, Q. Xue, L. Zhao, Y. Wu, A new type of bilayer dural substitute candidate made up of modified chitin and bacterial cellulose, Carbohydr. Polym. 256 (2021) 117577, https://doi.org/10.1016/j.carbpol.2020.117577.

[15] E.E. Dafford, P.A. Anderson, Comparison of dural repair techniques, Spine J. 15 (5) (2015) 1099–1105, https://doi.org/10.1016/j.spinee.2013.06.044.

[16] E.H. Choi, A.Y. Chan, N.J. Brown, B.V. Lien, R. Sahyouni, A.K. Chan, J. Roufail, M. Y. Oh, Effectiveness of repair techniques for spinal dural tears: a systematic review, World Neurosurg. 149 (2021) 140–147, https://doi.org/10.1016/j.wneu.2021.02.079.

[17] Q. Zhou, H. Kang, M. Bielec, X. Wu, Q. Cheng, W. Wei, H. Dai, Influence of different divalent ions cross-linking sodium alginate-polyacrylamide hydrogels on antibacterial properties and wound healing, Carbohydr. Polym. 197 (2018) 292–304, https://doi.org/10.1016/j.carbpol.2018.05.078.

[18] J. Li, A.D. Celiz, J. Yang, Q. Yang, I. Wamala, W. Whyte, B.R. Seo, N.V. Vasilyev, J. J. Vlassak, Z. Suo, et al., Tough adhesives for diverse wet surfaces, Science 357 (6349) (2017) 378–381, https://doi.org/10.1126/science.aah6362.

[19] T.P.C. van Doormaal, M.R. Germans, M. Sie, B. Brouwers, J. Fierstra, P. Depauw, P. A. Robe, L. Regli, Single-arm, open-label, multicenter study to evaluate the safety and performance of dura sealant patch in reducing cerebrospinal fluid leakage following elective cranial surgery: the ENCASE trial study protocol, Neurosurgery 86 (2) (2020) E203–E208, https://doi.org/10.1093/neuros/nyz396.

[20] F.M. Lima, F.C. Pinto, B.L. Andrade-da-Costa, J.G. Silva, O. Campos Junior, J. L. Aguiar, Biocompatible bacterial cellulose membrane in dural defect repair of rat, J. Mater. Sci. Mater. Med. 28 (3) (2017) 37, https://doi.org/10.1007/s10856-016-5828-9.

[21] A. Kinaci, S. van Thoor, S. Redegeld, M. Tooren, T.P.C. van Doormaal, Ex vivo evaluation of a multilayered sealant patch for watertight dural closure: cranial and spinal models, J. Mater. Sci. Mater. Med. 32 (8) (2021) 85, https://doi.org/10.1007/s10856-021-06552-4.

[22] J.F. Patrick, M.J. Robb, N.R. Sottos, J.S. Moore, S.R. White, Polymers with autonomous life-cycle control, Nature 540 (7633) (2016) 363–370, https://doi.org/10.1038/nature21002.

[23] C. Persson, S. Evans, R. Marsh, J.L. Summers, R.M. Hall, Poisson's ratio and strain rate dependency of the constitutive behavior of spinal dura mater, Ann. Biomed. Eng. 38 (3) (2010) 975–983, https://doi.org/10.1007/s10439-010-9924-6.

[24] D.J. Patin, E.C. Eckstein, K. Harum, V.S. Pallares, Anatomic and biomechanical properties of human lumbar dura mater, Anesth. Analg. 76 (3) (1993) 535–540, https://doi.org/10.1213/00000539-199303000-00014.

[25] E. Saygili, E. Kaya, E. Ilhan-Ayisigi, P. Saglam-Metiner, E. Alarcin, A. Kazan, E. Girgic, Y.W. Kim, K. Gunes, G.G. Eren-Ozcan, et al., An alginate-poly (acrylamide) hydrogel with TGF-beta3 loaded nanoparticles for cartilage repair: biodegradability, biocompatibility and protein adsorption, Int. J. Biol. Macromol. 172 (2021) 381–393, https://doi.org/10.1016/j.ijbiomac.2021.01.069.

[26] C.R. Arciola, D. Campoccia, L. Montanaro, Implant infections: adhesion, biofilm formation and immune evasion, Nat. Rev. Microbiol. 16 (7) (2018) 397–409, https://doi.org/10.1038/s41579-018-0019-y.

[27] W. Wang, Q. Meng, Q. Li, J. Liu, M. Zhou, Z. Jin, K. Zhao, Chitosan derivatives and their application in biomedicine, Int. J. Mol. Sci. (2) (2020) 21, https://doi.org/10.3390/ijms21020487.

[28] T. Xu, M. Xin, M. Li, H. Huang, S. Zhou, Synthesis, characteristic and antibacterial activity of N,N,N-trimethyl chitosan and its carboxymethyl derivatives, Carbohydr. Polym. 81 (4) (2010) 931–936, https://doi.org/10.1016/j.carbpol.2010.04.008.

[29] Y. Song, S. Li, B. Song, Y. Zhang, W. Gao, N. Li, K. Fan, J. Ma, The pathological changes in the spinal cord after dural tear with and without autologous fascia repair, Eur. Spine J. 23 (7) (2014) 1531–1540, https://doi.org/10.1007/s00586-014-3326-7.

[30] J. Trager, K. Widder, A. Kerth, G. Harauz, D. Hinderberger, Effect of cholesterol and myelin basic protein (MBP) content on lipid monolayers mimicking the cytoplasmic membrane of myelin, Cells 9 (3) (2020), https://doi.org/10.3390/cells9030529.

[31] D. Bartholdi, M.E. Schwab, Oligodendroglial reaction following spinal cord injury in rat: transient upregulation of MBP mRNA, Glia 23 (3) (1998) 278–284, https://doi.org/10.1002/(sici)1098-1136(199807)23:3<278::aid-glia10>3.0.co;2-q.

[32] C. Iannotti, Y.P. Zhang, L.B. Shields, Y. Han, D.A. Burke, X.M. Xu, C.B. Shields, Dural repair reduces connective tissue scar invasion and cystic cavity formation after acute spinal cord laceration injury in adult rats, J. Neurotrauma 23 (6) (2006) 853–865, https://doi.org/10.1089/neu.2006.23.853.

[33] J.E. Herrmann, T. Imura, B. Song, J. Qi, Y. Ao, T.K. Nguyen, R.A. Korsak, K. Takeda, S. Akira, M.V. Sofroniew, STAT3 is a critical regulator of astrogliosis

and scar formation after spinal cord injury, J. Neurosci. 28 (28) (2008) 7231–7243, https://doi.org/10.1523/JNEUROSCI.1709-08.2008.

[34] D. Li, X. Liu, T. Liu, H. Liu, L. Tong, S. Jia, Y.F. Wang, Neurochemical regulation of the expression and function of glial fibrillary acidic protein in astrocytes, Glia 68 (5) (2020) 878–897, https://doi.org/10.1002/glia.23734.

[35] K. Ohsawa, Y. Imai, Y. Sasaki, S. Kohsaka, Microglia/macrophage-specific protein Iba1 binds to fimbrin and enhances its actin-bundling activity, J. Neurochem. 88 (4) (2004) 844–856, https://doi.org/10.1046/j.1471-4159.2003.02213.x.

[36] M. Mandwie, J.A. Piper, C.A. Gorrie, K.A. Keay, G. Musumeci, G. Al-Badri, A. Castorina, Rapid GFAP and Iba1 expression changes in the female rat brain following spinal cord injury, Neural Regen. Res. 17 (2) (2022) 378–385, https://doi.org/10.4103/1673-5374.317982.

[37] H. Zeng, N. Liu, Y.Y. Yang, H.Y. Xing, X.X. Liu, F. Li, G.Y. La, M.J. Huang, M. W. Zhou, Lentivirus-mediated downregulation of alpha-synuclein reduces neuroinflammation and promotes functional recovery in rats with spinal cord injury, J. Neuroinflammation 16 (1) (2019) 283, https://doi.org/10.1186/s12974-019-1658-2.

[38] F. Richter, G. Natura, S. Loser, K. Schmidt, H. Viisanen, H.G. Schaible, Tumor necrosis factor causes persistent sensitization of joint nociceptors to mechanical stimuli in rats, Arthritis Rheum. 62 (12) (2010) 3806–3814, https://doi.org/10.1002/art.27715.

[39] J.R. Vane, Y.S. Bakhle, R.M. Botting, Cyclooxygenases 1 and 2, Annu. Rev. Pharmacol. Toxicol. 38 (1998) 97–120, https://doi.org/10.1146/annurev.pharmtox.38.1.97.

[40] X.C. Zhang, V. Kainz, R. Burstein, D. Levy, Tumor necrosis factor-alpha induces sensitization of meningeal nociceptors mediated via local COX and p38 MAP kinase actions, Pain 152 (1) (2011) 140–149, https://doi.org/10.1016/j.pain.2010.10.002.

[41] E.J. Bowen, T.W. Schmidt, C.S. Firm, A.F. Russo, P.L. Durham, Tumor necrosis factor-alpha stimulation of calcitonin gene-related peptide expression and secretion from rat trigeminal ganglion neurons, J. Neurochem. 96 (1) (2006) 65–77, https://doi.org/10.1111/j.1471-4159.2005.03524.x.

[42] X. Jin, RWt Gereau, Acute p38-mediated modulation of tetrodotoxin-resistant sodium channels in mouse sensory neurons by tumor necrosis factor-alpha, J. Neurosci. 26 (1) (2006) 246–255, https://doi.org/10.1523/JNEUROSCI.3858-05.2006.

[43] C.I. Svensson, T.L. Yaksh, The spinal phospholipase-cyclooxygenase-prostanoid cascade in nociceptive processing, Annu. Rev. Pharmacol. Toxicol. 42 (2002) 553–583, https://doi.org/10.1146/annurev.pharmtox.42.092401.143905.